nature communications

Article

https://doi.org/10.1038/s41467-024-51302-z

# Timing the first emergence and disappearance of global water scarcity

Received: 26 December 2022

Accepted: 5 August 2024

Published online: 20 August 2024

Check for updates

Junguo Liu[1,2,11] ✉, Delong Li[3,4,11], He Chen[3], Hong Wang[3], Yoshihide Wada[5], Matti Kummu[6], Simon Newland Gosling[7], Hong Yang[8], Yadu Pokhrel[9] & Philippe Ciais[10]

Alleviating water scarcity is at the core of Sustainable Development Goal 6. Yet the timing of water scarcity in its onset and possible relief in different regions of the world due to climate change and changing human population dynamics remains poorly investigated. Here we assess the timing of the first emergence of water scarcity (FirstWS) and disappearance of water scarcity (EndWS), by using ensembles of simulations with six Global Hydrological Models under two representative concentration pathways (i.e., RCP2.6, RCP6.0) combined with two shared socioeconomic pathways (i.e., SSP2, SSP3) for 1901–2090. Historically (1901–2020), FirstWS occurred predominantly in Asia (e.g., China and India) and Africa (e.g., East Africa); the peak time of emerging water scarcity began around the 1980s. Under all the four future RCPs-SSPs scenarios (2021–2090), FirstWS will likely occur mainly in some regions of Africa, for which the newly added area is double that in Asia. On the other hand, EndWS will mostly occur in China after 2050, primarily due to the projected declining population. We, therefore, call for specific attention and effort to adapt to the looming water scarcity in Africa.

The World Economic Forum 2020 has ranked the water crisis as the paramount social risk of this decade[1]. Managing water resources is the core pillar for addressing the most urgent challenges[2] and achieving sustainable development[3] in the Anthropocene. Due to intensifying climate change and regional population growth, the world now faces burgeoning water scarcity problems, defined for the purposes of this study as freshwater resource availability per capita below a certain threshold[4]. An expanding body of literature has examined how changes in climatic and societal factors[5] influence water availability[6,7]. They conclude that climate change and human interventions have profoundly altered the terrestrial water cycle and global water resources, adversely impacting water scarcity[8–10].

Existing global-scale assessments have examined the spatial distribution of water scarcity and the number of people affected by it[10,11] for the historical[12] and future[13,14] periods. However, there has yet to be a comprehensive and worldwide analysis of the occurrence and projected onset of water scarcity, as well as its potential disappearance, between 1901 and the 2090 s. This is particularly important when considering different scenarios of future population growth and climate change. By knowing when, where, and how many people are exposed to water scarcity, we can better understand the evolution and

[1]Yellow River Research Institute, North China University of Water Resources and Electric Power, Zhengzhou, China. [2]Henan Provincial Key Laboratory of Hydrosphere and Watershed Water Security, North China University of Water Resources and Electric Power, Zhengzhou, China. [3]School of Environmental Science and Engineering, Southern University of Science and Technology, Shenzhen, China. [4]Institute of Geographic Sciences and Natural Resources Research, Chinese Academy of Sciences, Beijing, China. [5]Biological and Environmental Science and Engineering Division, King Abdullah University of Science and Technology, Thuwal, Saudi Arabia. [6]Water & Development Research Group, Aalto University, Espoo, Finland. [7]School of Geography, University of Nottingham, Nottingham, UK. [8]2W2W Consulting, GmbH, Duebendorf, Switzerland. [9]Department of Civil and Environmental Engineering, Michigan State University, East Lansing, MI, USA. [10]Laboratoire des Sciences du Climat et de l'Environnement, CEA CNRS UVSQ Gif-sur-Yvette, France. [11]These authors contributed equally: Junguo Liu, Delong Li. ✉e-mail: junguo.liu@gmail.com

scale of the problem and inform policymakers to formulate strategies to adapt to and mitigate the situation. To address the current gap in knowledge, we have conducted a new global-scale analysis that examines the emergence and disappearance of water scarcity on a temporal basis. Specifically, we define the "FirstWS" as the initial year when the per-capita water availability at the grid scale falls below the 1000 $m^3$/person/year threshold[4] for a minimum of five consecutive years[15] between 1901 to 2090. Additionally, we define the "EndWS" as the year when the water scarcity is relieved for a continuous period of five years or more, and the scarcity-free state remains until the end of the 21st century (Fig. 1). In this study, we introduce a novel approach to identifying the "FirstWS" and "EndWS" on a global scale with a bicentennial perspective (see Methods and Supplementary Fig. 1).

As many as 150 different indicators of water scarcity have been developed[16]. Here, we use the per-capita water availability metric, also called the Falkenmark index[4,17,18] (see SI "Falkenmark Indicator for water scarcity assessment"). It is widely applied due to its simplicity and low input data requirement[19,20]. Furthermore, this indicator does not require data on water use, which is highly uncertain under future scenarios[4,13,20].

The present study covers 1901–2090, split into the historical period (1901–2020) and the future (2021–2090). The assessment is based on overall water availability and population on a global scale and at a spatial resolution of 0.5° × 0.5° (about 50 km × 50 km for each grid cell near the equator). Water availability, defined here as the amount of renewable blue freshwater (surface and groundwater) on an annual basis, was derived from six Global Hydrological Models (GHMs) conducted under the Inter-Sectoral Impact Model Inter-comparison Project phase 2b (ISIMIP2b)[9]. Each GHM was forced with bias-adjusted climate simulations from four General Circulation Models (GCMs) for the historical and future periods, yielding 24 GHM-GCM combinations. These 24 GHM-GCM combinations were selected due to the data availability (Supplementary Table 1). The simulations of freshwater in the future were based on two representative concentration pathways (RCPs): RCP2.6 (low-emission scenario) and RCP6.0 (medium-emission scenario). We used total runoff—the sum of surface runoff (overland flow) and lateral flow (including the groundwater recharge)—as a proxy for freshwater availability. Two shared socioeconomic pathways were used to estimate changes in future human population projections:

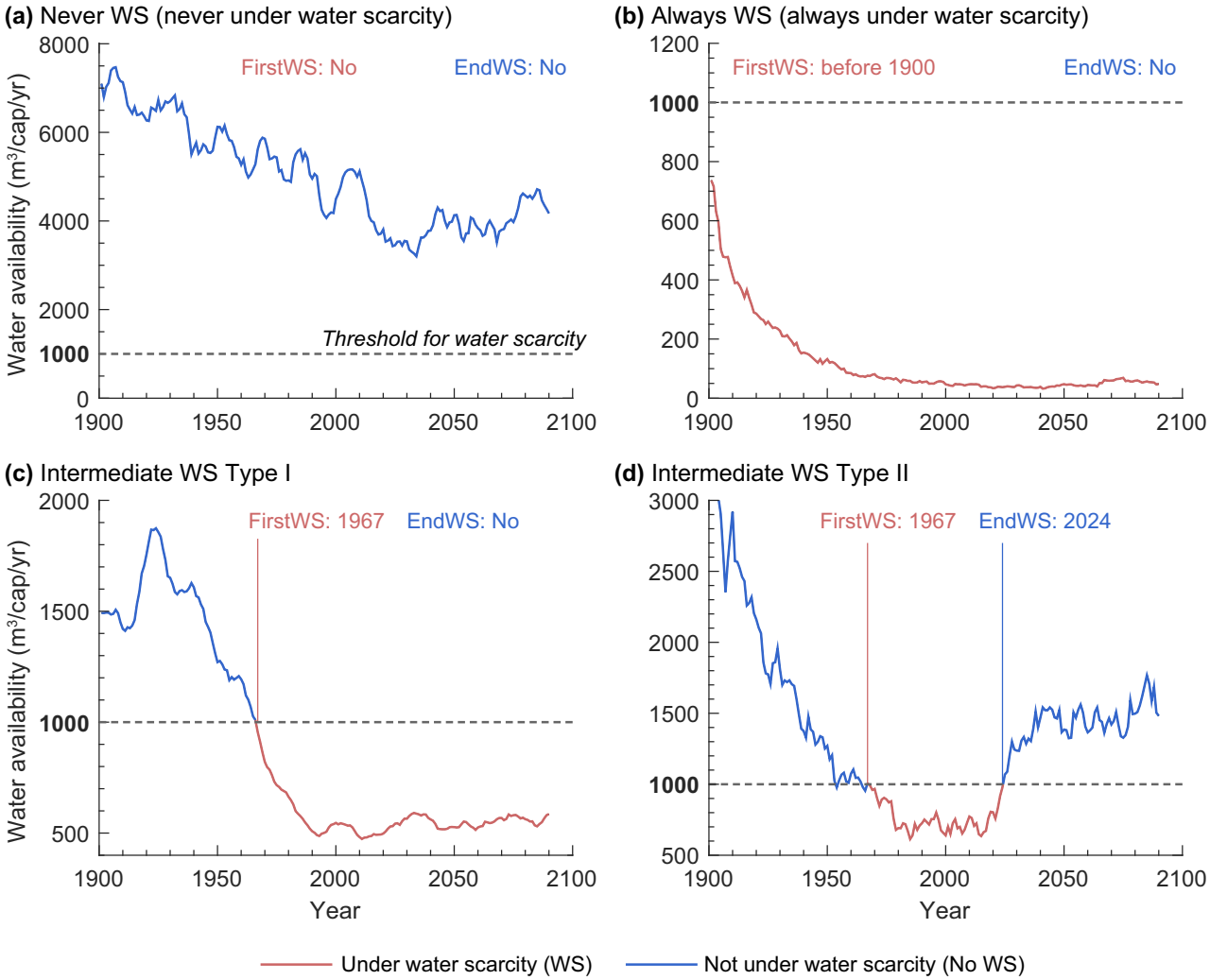


**Fig. 1 | Schematic diagram depicting four different patterns used to identify the FirstWS and EndWS. a** The 'Never WS' condition denotes the absence of water scarcity (WS) during the entire study period (i.e., nonexistent FirstWS and EndWS). **b** The 'Always WS' refers to the condition where WS occurred before the 20th century (i.e., FirstWS before 1901) and lasted the entire period; an EndWS cannot be identified. **c** The 'Intermediate WS Type I' pattern corresponds to a condition whereby WS occurs intermittently yet continues until the late phase of the study period, i.e., an EndWS can not be identified within the study period. **d** In the 'Intermediate WS Type II' condition, the water scarcity also occurs intermittently but it disappears in the late phase of the study period; both its FirstWS and EndWS can be identified. The "FirstWS" is defined as the initial year when the per-capita water availability at the grid scale falls below the 1000 $m^3$/person/year threshold for a minimum of five consecutive years between 1901 to 2090. The "EndWS" is defined as the first year when the water scarcity is relieved for a continuous period of five years or more, and the scarcity-free state remains until the end of the 21st century.

https://doi.org/10.1038/s41467-024-51302-z

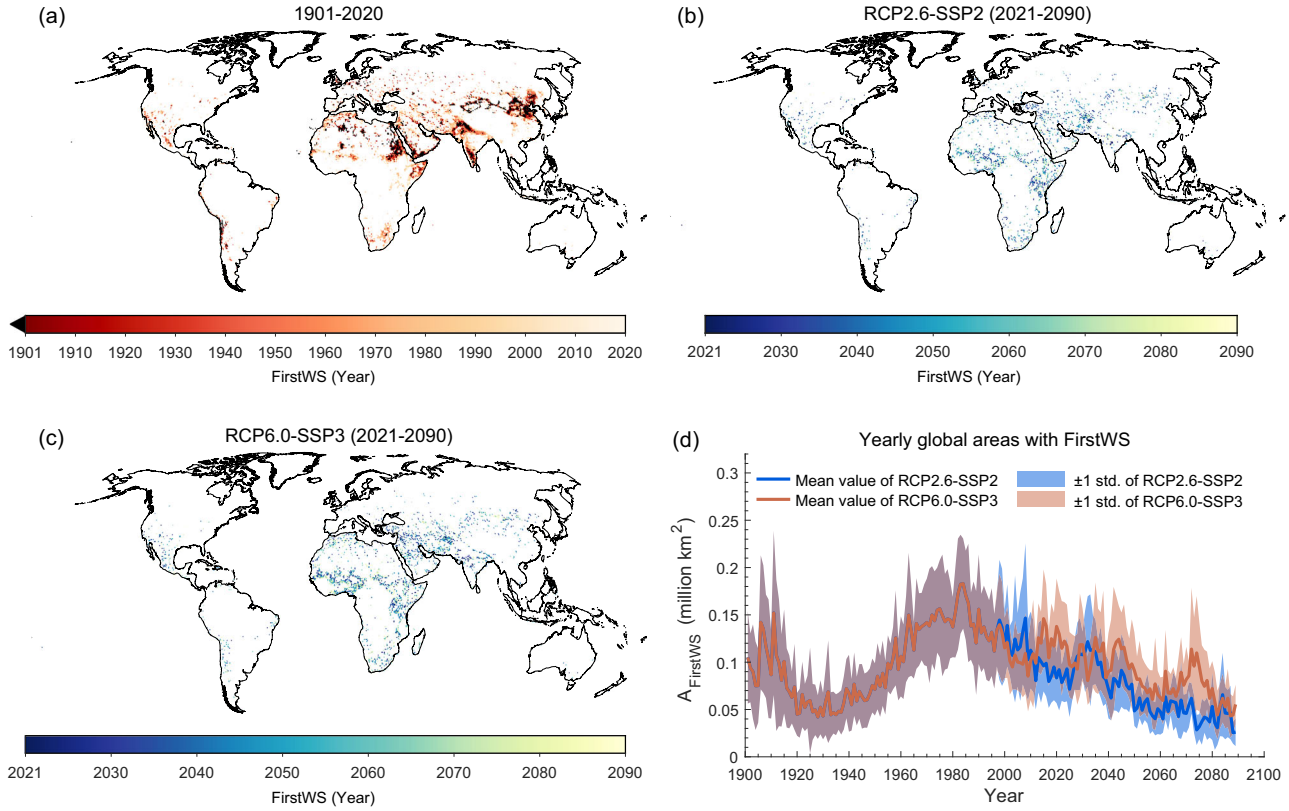


**Fig. 2 | Spatial distributions of multi-model ensemble median of FirstWS for RCP2.6-SSP2 and RCP6.0-SSP3 scenarios.** The median year of FirstWS projected is based on 24 GHM-GCM combinations for the (**a**) historical period (1901–2020) and (**b**) future period (2021–2090) under the RCP2.6-SSP2 combination; and for the (**c**) future period under the RCP6.0-SSP3 combination. **d** Global area in a given year when the FirstWS is identified ($A_{FirstWS}$). In **a**, black indicates where water scarcity occurred before 1901, and white shows that water scarcity never happened in the historical period. In **a**, **b**, **c**, any pixel with low model agreement (FirstWS occurs for less than one-third (i.e., <8) of all the GHM-GCM combinations) are shown in white. Note that the FirstWS was the median year of 24 model (**a**–**c**), while the areas of yearly FirstWS (**d**) were the mean and one standard deviation. The "FirstWS" is defined as the initial year when the per-capita water availability at the grid scale falls below the 1000 $m^3$/person/year threshold for a minimum of five consecutive years between 1901 to 2090.

SSP2 (middle of the road, medium population growth) and SSP3 (regional rivalry, highest population growth).

## Results

### Global water scarcity patterns

Four patterns of water scarcity are synthesized in Fig. 1 to illustrate the identification of FirstWS and EndWS. A summary of these four patterns based on the 24 GHM-GCM simulations for the entire study period 1901–2090 and under the RCP2.6-SSP2 combination is presented in Supplementary Table 2. During the study period, over half of the globe's terrestrial area (52.9% ± 4.9%; mean ± standard deviation of 24 model combinations, the same hereafter) never encounters water scarcity ('Never WS', Fig. 1a). In contrast, areas always enduring water scarcity ('Always WS', Fig. 1b) account for only 4.1% ± 3.5% of the globe's terrestrial area. We distinguish two patterns for 'Intermediate WS'. For type I, water scarcity occurs from a specific year until the end of the study period (Fig. 1c); this pattern covers 12.1% ± 2.2% of the globe's terrestrial area. For type II, water scarcity occurs intermittently but does not persist until the study period's end; this pattern appears in 4.9% ± 1.4% of the globe's terrestrial area. Since this study aims to identify the FirstWS and EndWS, the intermediate water scarcity areas (Type I and II) are of primary concern.

### A bicentennial perspective of FirstWS

FirstWS varied considerably among the 24 different GHM-GCM combinations (Supplementary Fig. 2); hence, we used the multi-model ensemble median of FirstWS from all GHM-GCM combinations. Figure 2 shows the RCP2.6-SSP2 and RCP6.0-SSP3 scenarios; refer to Supplementary Fig. 3 for the RCP2.6-SSP3 and RCP6.0-SSP2 scenarios). FirstWS was detected prior to the early 20$^{th}$ century in parts of East Asia (mainly in the northern part of China), South Asia (mainly in the southern and northern parts of India, and eastern parts of Pakistan), Western Asia (Iran and Saudi Arabia), and North Africa (northern parts of Sudan) (Fig. 2a). By 2020, the global total area of $A_{FirstWS}$ reached 12.34 ± 2.55 million $km^2$, accounting for 8% ± 2% of the world's terrestrial area, respectively (Table 1). Asia and Africa are two continents with a dominant occurrence of FirstWS during the historical period (Fig. 2; Supplementary Fig. 3), which accounted for 46% ± 6% and 33% ± 4% of the world's total areas with emerging water scarcity, respectively (Supplementary Table 3). In the future, new areas where water scarcity emerges will likely be predominantly in the African continent, particularly in East Africa (Ethiopia), West Africa (Nigeria), and North Africa (Sudan) (Figs. 2b, 2c). For the pooled areas experiencing new water scarcity in the future (2021–2090) under the RCP2.6-SSP2 scenario, Africa and Asia are also the largest values of total new emerging water scarcity areas, which account for 46% ± 6% and 33% ± 4% of the world's total (Supplementary Table 3). The total areas with new emerging water scarcity in Africa is more than double the Asia's (Supplementary Table 3). Thus, looking ahead, FirstWS is likely to be more prevalent in Africa than in Asia (Fig. 2b, c).

At the national level, we identified the top ten countries with the largest $A_{FirstWS}$ between 1901 and 2090 (Supplementary Table 4) and found China and India are the two countries with the largest areas with $A_{FirstWS}$ in the historical period, amounting to 27% ± 4% and 24% ± 4% of

https://doi.org/10.1038/s41467-024-51302-z

**Table 1 | The global cumulative areas and the number of people crossing the FirstWS and EndWS in the historical (1901–2020) and future (2021–2090) periods**

| Cumulative areas or population | Historical (1901–2020) | Future (2021–2090) | | | |
|---|---|---|---|---|---|
| | | RCP2.6-SSP2 | RCP6.0-SSP2 | RCP2.6-SSP3 | RCP6.0-SSP3 |
| $\sum A_{FirstWS}$ (million km$^2$) | 12.34 ± 2.55 | 4.52 ± 0.61 | 4.76 ± 1.06 | 5.90 ± 0.69 | 6.00 ± 1.09 |
| $\sum A_{EndWS}$ (million km$^2$) | 0.45 ± 0.22 | 3.92 ± 1.25 | 4.13 ± 0.94 | 3.28 ± 1.16 | 3.42 ± 0.92 |
| $\sum P_{FirstWS}$ (billion) | 1.44 ± 0.13 | 0.78 ± 0.088 | 0.76 ± 0.13 | 1.19 ± 0.16 | 1.11 ± 0.18 |
| $\sum P_{EndWS}$ (billion) | 0.02 ± 0.007 | 0.54 ± 0.097 | 0.65 ± 0.096 | 0.45 ± 0.081 | 0.53 ± 0.099 |

For future scenarios, the emission scenarios are RCP2.6 and RCP6.0, while the population scenarios are SSP2 and SSP3. The results shown are the mean of 24 model ensembles (± 1 standard deviation). The "FirstWS" is defined as the initial year when the per-capita water availability at the grid scale falls below the 1000 m$^3$/person/year threshold for a minimum of five consecutive years between 1901 to 2090. The "EndWS" is defined as the first year when the water scarcity is relieved for a continuous period of five years or more, and the scarcity-free state remains until the end of the 21st century.

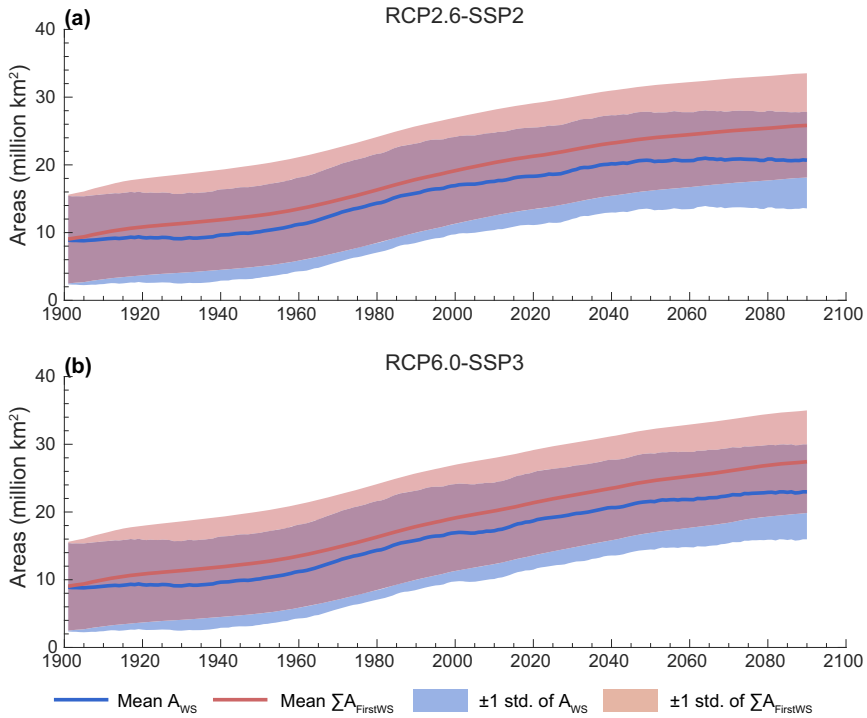


**Fig. 3 | Multi-model ensemble means of global water scarcity areas ($A_{WS}$) and the accumulated newly emerging water scarcity areas before a given year ($\sum A_{FirstWS}$) from 1901 to 2090. a** Water availability (RCP2.6), population (SSP2); **b** water availability (RCP6.0), population (SSP3). Shading shows the standard deviation (std) of $A_{ws}$ and $\sum A_{FirstWS}$ for the 24 GHM-GCM combinations. The "FirstWS" is defined as the initial year when the per-capita water availability at the grid scale falls below the 1000 m$^3$/person/year threshold for a minimum of five consecutive years between 1901 to 2090.

the world's total, respectively (Supplementary Tables 5). In the future, the countries with the largest areas with $A_{FirstWS}$ will be Nigeria and India, respectively, accounting for 8% ± 2% and 7% ± 3% of the world's total areas with $A_{FirstWS}$ under RCP2.6-SSP2 (Supplementary Table 5). By then, China will only comprise 2% ± 1% of the world's total areas with $A_{FirstWS}$ under the RCP2.6-SSP2 scenario.

We used $A_{FirstWS}$ to indicate the annual total area where new water scarcity emerged. On a global scale, $A_{FirstWS}$ has increased since the 1930s but peaked around the 1980s (Fig. 2d). For the different continents, generally, the $A_{FirstWS}$ initially declined but rebounded to a peak, after which it declined again, with this pattern most pronounced in Asia, Africa, and North America (Supplementary Fig. 4). We compared the top ten countries with largest cumulative areas of FirstWS (Supplementary Table 4). Not surprisingly, the trend in $A_{FirstWS}$ varies among countries (Supplementary Fig. 5). However, India and China show similar trends in their $A_{FirstWS}$ before the 1970s, in China it began to decrease in the 1990s. In contrast, in India, it continually rose until the 2020 s. While the peaks of $A_{FirstWS}$ differ among countries, such peaks are primarily found in the 1980s and 1990s, e.g., in the US, China, Pakistan, and Iran (Supplementary Fig. 5).

## The cumulative area with emerging water scarcity

In any year, we can estimate the areas with water scarcity using the water scarcity threshold (i.e. per capita available water is lower than 1000 m$^3$/person/year in this study). However, current water scarcity state does not reflect the regions where water scarcity was encountered in the past but has been relieved later. We compared $\sum A_{FirstWS}$ (the accumulated newly emerging water scarcity areas before a given year) to traditional $A_{WS}$ (areas with water scarcity state in a given year) (Fig. 3). $A_{WS}$ is equal to or smaller than $\sum A_{FirstWS}$ because a region may alleviate from water scarcity after a specific year (e.g., Fig. 1d). During the historical period, $A_{WS}$ and $\sum A_{FirstWS}$ both increased (Fig. 3). In 2020, although $\sum A_{FirstWS}$ will continue to increase in the future under all the RCP-SSP scenario combinations (Fig. 3 for the RCP2.6-SSP2 and RCP6.0-SSP3 scenarios; Supplementary Fig. 6 for the RCP2.6-SSP3 and RCP6.0-SSP2 scenarios), $A_{WS}$ may peak around 2050 s under the

https://doi.org/10.1038/s41467-024-51302-z

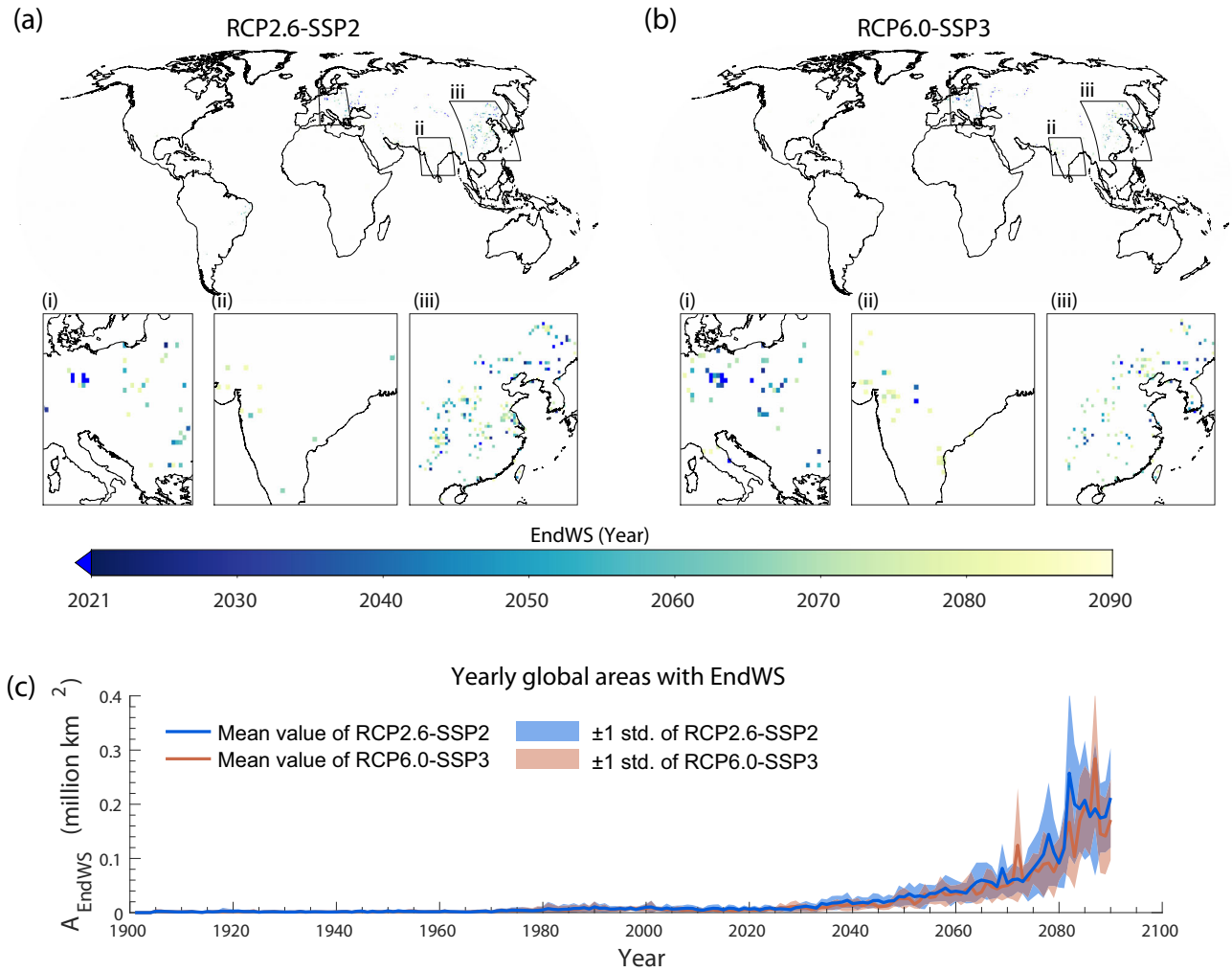


**Fig. 4 | Disappearance time of water scarcity (EndWS).** Panels **a**, **b** show the spatial distributions of the multi-model ensemble median year of EndWS under RCP6.0-SSP2 and RCP2.6-SSP3, respectively. White coloring indicates where EndWS will never occur before 2090. Shown in **c** is the temporal evolution of $A_{EndWS}$. Noted that the EndWS was the median year of 24 models' value (**a**, **b**), while the areas of yearly EndWS (**c**) were the mean value and one standard deviation. The "EndWS" is defined as the first year when the water scarcity is relieved for a continuous period of five years or more, and the scarcity-free state remains until the end of the 21st century.

RCP2.6-SSP2 scenarios. The difference between $\sum A_{FirstWS}$ and $A_{WS}$ is the greatest under RCP2.6-SSP2 vis-à-vis the other scenarios (Fig. 3; Supplementary Fig. 6). This is because water scarcity could be relieved mainly due to declining human population in the future, particularly so under RCP2.6-SSP2. The gap between $\sum A_{FirstWS}$ and $A_{WS}$ will continue to increase after 2060 s. This is because some regions that ever underwent water scarcity will be relieved. Thus, the disappearing water scarcity should also be investigated.

## Spatial distribution of EndWS

We noted above that some regions would see an alleviation in their future water scarcity (Fig. 1d) due to greater water availability per capita (Supplementary Fig. 7). The first disappearing time of water scarcity (EndWS) varied greatly among the 24 different GHM-GCM combinations (Supplementary Fig. 8). The median value of EndWS of 24 GHM-GCM combinations showed that disappearance of water scarcity is most pronounced in East Asia (China) and Central Europe (Fig. 4a, b; Supplementary Fig. 9; Supplementary Fig. 10; Supplementary Fig. 11). We use $A_{EndWS}$ to indicate the annual total area with newly disappeared water scarcity. On a global level, there is a general increasing trend in $A_{EndWS}$, which strengthens into the future but harbors considerable uncertainty based on the 24 GHM-GCM models regarding future water availability and population sizes (Fig. 4c).

We use $\sum A_{EndWS}$ to show the total area of grid cells in which water scarcity ended in or before a given year within a particular region. In the historical period, $\sum A_{EndWS}$ is extremely small, but in the future, it increases substantially, to 3.9 ± 1.3 and 3.4 ± 0.9 million km$^2$ under RCP2.6-SSP2 and RCP6.0-SSP3, respectively(Table 1). The cumulative areas where water scarcity will be relieved in the future are mainly in Asia. Under the RCP2.6-SSP2 scenario, Asia will account for 55% ± 14% of the globe's terrestrial area that becomes free of water scarcity. In contrast, Africa only accounts for 14% ±10% (Supplementary Table 6). We further identified the top ten countries with the largest $A_{EndWS}$ between 1901 and 2090 (Supplementary Table 7). Water scarcity's disappearance will be dominant in China, primarily due to the projected decline in its population, thereby constituting 24% ± 7% of the global $\sum A_{EndWS}$; in contrast, India will account for only 8% ± 4% of it (Supplementary Table 8).

## The cumulative population affected by FirstWS and EndWS

We assessed the size of the global cumulative population when it crossed the FirstWS ($\sum P_{FirstWS}$) and EndWS ($\sum P_{EndWS}$) (Table 1). The $\sum P_{FirstWS}$ in the historical period exceeded that in the future period: it

https://doi.org/10.1038/s41467-024-51302-z

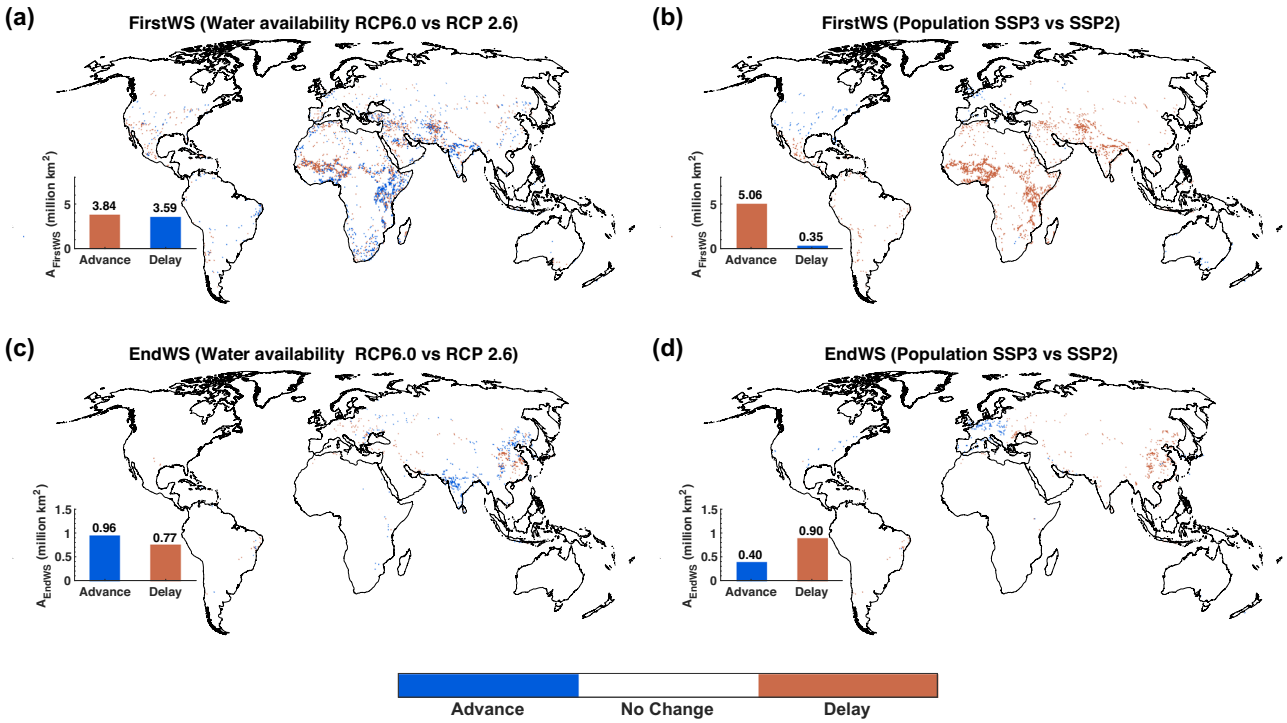


**Fig. 5 | Impact of population and climate change scenarios upon water scarcity.** The advance or delay in FirstWS between (**a**) RCP6.0 and RCP2.6 under the SSP2 population scenario and between (**b**) SSP3 and SSP2 under the RCP2.6 emission scenario. The advance or delay of EndWS between (**c**) RCP6.0 and RCP2.6 under the SSP2 population scenario and between (**d**) SSP3 and SSP2 under the RCP2.6 climate change scenario. The figures under each bar indicate the total areas (million km$^2$). The "FirstWS" is defined as the initial year when the per-capita water availability at the grid scale falls below the 1000 m$^3$/person/year threshold for a minimum of five consecutive years between 1901 to 2090. The "EndWS" is defined as the first year when the water scarcity is relieved for a continuous period of five years or more, and the scarcity-free state remains until the end of the 21st century.

was 1.44 ± 0.13 billion in the historical period (1901-2020) and 0.78 ± 0.099 and 1.11 ± 0.18 billion in the future under RCP2.6-SSP2 and RCP6.0-SSP3, respectively. In the historical period, the $\sum P_{FirstWS}$ of Asia (0.95 ± 0.09 billion) surpassed that of Africa (0.19 ± 0.02 billion) (Supplementary Table 9). In the future, Africa and Asia have the highest $\sum P_{FirstWS}$ among all continents under all four scenario combinations (Supplementary Table 9). At the country level, China and India had the highest $\sum P_{FirstWS}$ in the historical period, accounting for 36% ± 5% and 43% ± 6% of the world's $\sum P_{FirstWS}$, respectively (Supplementary Table 10). However, the $\sum P_{FirstWS}$ of China will be very low in the future, corresponding to merely one-fifteenth that of India under the RCP2.6-SSP2 scenario combination (Supplementary Table 10).

Only 18.1 ± 6.1 million people were relieved from water scarcity in the historical period. But the $\sum P_{EndWS}$ in the future would reach 183.5 ± 22.9 million and 95.0 ± 211.0 million under RCP2.6-SSP2 and RCP6.0-SSP3, respectively. Continentally, the future $\sum P_{EndWS}$ will be the largest for Asia (67% ± 7% of the global $\sum P_{EndWS}$ under RCP2.6-SSP2), but the least for Africa (Supplementary Table 11). On the other hand, China will likely have the highest $\sum P_{EndWS}$ among all countries in the future (Supplementary Table 12).

## Impact of future population growth and climate change on FirstWS and EndWS

To investigate the extent to which future population and climate change scenarios may affect FirstWS, we compared its difference between climate change scenarios by fixing the population scenarios and, likewise, compared its difference between population scenarios by fixing the climate change scenarios (Fig. 5). A delayed FirstWS and advanced EndWS would correspond to alleviated water scarcity. In contrast, the advanced FirstWS and delayed EndWS can be interpreted as aggravated water scarcity. When the population remains unchanged, under the RCP6.0 scenario, we find slightly more areas with delayed FirstWS compared with RCP2.6 (Fig. 5a). This is mainly because future global water availability is greater in the high emission scenario (RCP6.0) than low emission scenario (RCP2.6) (Supplementary Fig. 12). Yet the evolution of water availability is not even among different regions. Delayed FirstWS (blue bar in Fig. 5a) will occur in Southern Africa and South Asia (India) under RCP6.0 vis-à-vis RCP2.6 (Supplementary Fig. 13), while advanced FirstWS (red bar in Fig. 5a) will occur in Central Asia (Afghanistan) and West Africa (Sudan) due to less water availability there under RCP6.0. Concerning EndWS, we find more delayed areas in RCP6.0 in comparison with RCP2.6 (Fig. 5c). Advanced EndWS will arise in India, Europe, and Northeast China, but delayed EndWS will occur in South China (Fig. 5c) due to differential trends in regional water availability (Supplementary Fig. 14).

We kept the emission scenario unchanged (always RCP2.6) to demonstrate the impact of population alone on water scarcity. On a global scale, the future population under SSP3 is larger than that in SSP2 (Supplementary Fig. 15). High population growth could significantly aggravate water scarcity, which would manifest as advanced FirstWS (Fig. 5b) and delayed EndWS (Fig. 5d). However, the global population is not evenly distributed, in that, SSP3 still has fewer people in SSP2 for certain regions, such as Central Europe and North America (Supplementary Fig. 16; Supplementary Fig. 17). This variation leads to differences in how FirstWS and EndWS are advanced or delayed in individual regions as well as countries.

## Uncertainty in FirstWS and EndWS

The six Global Hydrological Models (GHMs) and four General Circulation Models (GCMs) are widely used to estimate global and local water resources[8,21–25]. While these models are widely used, the consistency from the GCMs and GHMs was relatively low

(Supplementary Fig. 18). The uncertainty among six GHMs was much higher than that of four GCMs (Supplementary Fig. 18). However, it is common practice in hydrological modeling to focus on the impact of the input scenarios (in this case, the representative concentration pathways and socioeconomic pathways) rather than the uncertainty of the model itself, especially at large scales[26,27]. By analyzing the impact of the input scenarios, we can gain valuable insights into the potential effects of different policy decisions or trends on the hydrological system, even if the exact values of the model output are uncertain.

Having devised the novel idea of FirstWS and EndWS, we recommend more local applications to consider the uncertainties of all considered hydrological models as there will be less computational demand. In the following, we provide a detailed discussion of the sources of the accounted-for uncertainties.

Further to the above considerations, we used a moving average analysis of the time series of freshwater availability to remove interannual variability. Our results are based on a water scarcity threshold of 1000 $m^3$ per person per year at pixel scale and an 11-year moving average window. Considering that there is little EndWS before 2020, we did not compare the EndWS between model and observations and only compared the consistency of FirstWS. Although the pattern of FirstWS varies among the 24 different GHM-GCM combinations (Supplementary Fig. 2), the 25–75% range of FirstWS projected by 24 GHM-GCM combinations was less than 50 years, especially in Asia (Supplementary Fig. 19). An alternative approach was also used to test the uncertainty of 24 GHM-GCM models. We first calculated the median freshwater resource of 24 GHM-GCM combinations and then estimated the final FirstWS, which generated a similar spatial pattern for FirstWS (Supplementary Fig. 20) compared to that shown in Fig. 2. Thus, the ensemble median of 24 GHM-GCM combinations provides a robust estimate of FirstWS. We further tested the sensitivity of moving average windows and the water scarcity threshold to FirstWS. Using a 5-year and 21-year moving average window yielded similar spatial patterns for FirstWS and trends in FirstWS (Fig. 2; Supplementary Fig. 21). Although the higher threshold moved FirstWS to occur earlier and the lower threshold postponed the occurrence of FirstWS, the trend and patterns in FirstWS were all consistent (Fig. 2; Supplementary Fig. 22).

Our FirstWS were calculated at the grid scale. As water resources can be redistributed and stored by human activities (e.g., dams and reservoirs), the grid scale calculation may overlook these effects. We, therefore, also conducted calculations at the watershed scale. This scale would, to a certain extent, dampen the effects of redistribution and storage within a watershed scale. We found that the FirstWS on the watershed scale (Supplementary Fig. 23) showed similar spatial patterns and trends to those at the grid scale (Fig. 2). However, differences are also significant. Overall, the curves for the grid scale are smoother than those for the watershed scale, which appeared rather 'spiky'. This is because when a whole watershed entered FirstWS at a particular year, its effect on the $A_{FirstWS}$ of that year would be more significant than when only individual grids in the watershed get into FirstWS at the time. Another noticeable feature is that for most of the historical period, the curve for the watershed scale is below the curve for the grid scale, while since approximately the 1960s, the two curves changed the position. This is because in the early period, there were only some spots with water scarcity, whereas the watershed as a whole is above the water scarcity threshold. In the later years, the watershed scale $A_{FirstWS}$ was generally higher than the grid scale $A_{FristWS}$. With population increases, watersheds on average could pass the water scarcity threshold, hence the whole watershed area was included in the $A_{FirstWS}$, despite there may be many sub-areas in the watershed having water resources above the threshold. In this study, we present the results from the grid scale as it can better capture the hot-spots areas with water scarcity locally.

Finally, we used other runoff data (G-RUN ensemble[28] between 1902 and 2019) to test the validity of our data sources. We found that the model estimates line up the result of G-RUN, especially in Africa, Central Asia, and West Asia (Supplementary Fig. 24). The trend of $A_{FirstWS}$ based on modelled data is similar to that of observations (Supplementary Fig. 24). Thus, our model can capture the signals of newly emerging water scarcity.

## Discussion

This study is the first to report the time of the emergence and disappearance of water scarcity at the global scale during the 20th and 21st centuries. While water scarcity has been widely documented and monitored with the regions and people around the globe suffering from water scarcity in real time[29], the FirstWS and EndWS in this study provide the key "window of opportunity"[30] for transitioning to sustainability, and water-related indicators for the efforts made to achieve the Paris Agreement's long-term temperature goal[31]. For example, we have more time to prepare for upcoming water scarcity regarding the FirstWS of 2050 relative to 2030.

Our EndWS presents the first spatially-explicit map of the timing for when a region begins to alleviate its water scarcity. For those regions with an EndWS in 2050, it suggests there are 30 years to go before water scarcity is reversed there. From the perspective of sustainable water resources management, the aim of a region that has no water scarcity should be to delay as much as possible its FirstWS or avoid it altogether. But a region that has encountered water scarcity should devote itself to advancing its EndWS. Our FirstWS and EndWS complement other water scarcity indicators[20] and provide additional information that is needed to formulate flexible, time-based, and site-based adaptive interventions. The concept developed, and approaches applied could help policy-makers formulate strategies to meet the more ambitious SDG 6.1 and 6.2 targets[32].

Our results for FirstWS showed that global water scarcity had risen and expanded since the 1930s and peaked around the 1980s (Fig. 2d), with very similar patterns in Asia and Africa. This pattern is best explained by the relatively slow increase in the global population between 1901 and the 1930s and its rapid growth, especially after World War II up to the 1980s (Supplementary Fig. 13). The 1950s is often seen as the beginning of the Anthropocene[24]. The high post-war population boom also led to a fast increase in $A_{FirstWS}$.

Although we found historically high water scarcity pressure in Asia and Africa, after 2020, the FirstWS is expected to happen principally in Africa (Fig. 2). The EndWS after 2020 would mainly be in Asia (Fig. 4), further implies water relief there, especially in China. More attention should be paid to preparing for the looming water scarcity in Africa, as the continent will face declining water availability and a growing population in tandem (Supplementary Fig. 12; Supplementary Fig. 15).

The relative influences of population and climate change (climate scenario) on FirstWS and EndWS vary among time periods and regions. The past trend of FirstWS is largely dominated by population size, but the future trend of FirstWS is driven by both population and climate change-induced water availability alterations. In the historical period, we found the pattern of $A_{FirstWS}$ similar to the increasing population trend (1901–2020) (Supplementary Fig. 13). In the future period, stark differences between the population scenarios are expected (Fig. 5). In this respect, however, the difference between the climate change scenarios is relatively small compared to that between the population scenarios (Fig. 5). Compared with population growth, climate change affects water availability on a more regional basis (Supplementary Fig. 12). Globally, the increase in total water availability will be greater for the high emission scenario (RCP6.0) than the low emission scenario (RCP2.6) (Supplementary Fig. 10). Thus, future water scarcity is expected to be alleviated with augmented global water availability (without considering weather fluctuations, which have been projected

to be extreme). However, the $\sum A_{FirstWS}$ under RCP6.0 will be larger than that under RCP2.6 from 2021 to 2090 (Table 1). This contradiction stems from regions with increasing global water availability (Supplementary Fig. 12) being mainly distributed in areas with rapid population growth (Supplementary Fig. 15).

While the FirstWS and EndWS provide valuable insights into assessing future water risks, there are some important considerations to acknowledge. Firstly, our assessment of water scarcity relied on the Falkenmark Indicator, which serves as a simplified measure for understanding water availability relative to population needs. However, it has limitations in capturing all dimensions of water scarcity, such as water quality, accessibility, and distribution. Other factors like regional characteristics, climate conditions, and water management practices also significantly influence water availability and usage patterns. The variations in water use efficiency and technologies across regions further impact the level of water scarcity experienced[33]. Therefore, it is crucial to recognize that a fixed threshold of 1000 $m^3$ per person per year may not adequately account for these variations. For example, countries like Israel and other developed nations with high-efficiency water use technologies may require lower thresholds to indicate water scarcity compared to regions employing less efficient practices[16]. Additionally, the influence of socio-economic development on water scarcity should be considered in assessments. Interpreting the threshold within the specific regional context and considering other relevant indicators and factors are essential for accurately evaluating water scarcity. Secondly, it is important to note that certain factors were not accounted for in this study, such as sectoral water use, environmental flow, water quality, and water technologies or related infrastructure. These factors were omitted since they would place excessive demands on input data which are often unavailable anyway[12,20,34]. Water availability in this study is the sum of renewable surface water and groundwater, a large portion of which is inaccessible to humans[35] due to water pollution, locations far from the point of demand, and a lack of adequate water infrastructure. Additionally, the limited data availability prevents us from pursuing an in-depth analysis of the impact of environmental flows on water scarcity[36,37].

Thirdly, whether the yearly FirstWS and EndWS correspond to the actual situation on the ground needs to be independently verified because GCM forcing from ISIMIP does not reproduce the decadal variability of climate as observed[38]. The substantial stochastic variability from each of the 24 GHM-GCM combinations may propagate much uncertainty, as would bringing in too many input variables, each with its error sources. Lastly, we did not account for the impact of human activities on water redistribution and storage, such as the significance and ubiquity of water management practices like dams and reservoirs, and long-distance water transfer dynamics[39]. One major issue not included in this analysis is the horizontal and seasonal redistribution and storage of water by human activities (e.g., dams and reservoirs). For example, in the western US many states are dependent on water generated by snowmelt from the Upper Colorado River basin. This water is stored in Lake Mead and Lake Powell and then allocated to stakeholders across thousands of square kilometers. In addition to local runoff, the inflows from upstream are important sources of water resources for the western US, and other regions. Veldkamp et al. [39] reveal that human interventions like land use changes, reservoirs, and water usage strongly impact water scarcity, with 8.8% of the global population experiencing worsened scarcity, while 8.3% benefit. They also find that positive effects occurred upstream, exacerbating water scarcity downstream as it travels. Zhao et al. [40] find that redistribution of water through physical and virtual flows alleviate water scarcity in several cities located in Northern China such as Beijing and Tianjing. We also did not consider refugees moving across regions and borders due to climate change impacts and other factors (e.g., regional conflicts and wars). All these caveats can be further addressed by including more modules, incorporating new and updated runoff and water consumption data, expressing water scarcity using a water use-to-availability ratio, or considering river discharge from upstream areas, as well as cross-border migration.

## Methods

### Data overview

Water availability was calculated from total runoff, which is the sum of surface runoff (overland flow) and subsurface runoff (including renewable groundwater). Runoff was simulated by six GHMs (CLM45, H08, LPJm, MATSIRO, PCR-GlobWB, WaterGAP2) that participated in the ISIMIP2b project (Supplementary Table 1). The GHMs used forcing data driven by four General Circulation Models (GCMs) (GFDL-ESM2M, HadGEM2-ES, IPSL-CM5A-LR, and MIROC5) in the Coupled Model Intercomparison Project Phase 5 (CMIP5)[29]. It has been proven the four selected GCMs mirrors the variability found in the entire ensemble in CMIP5, indicate a high level of representativeness[21]. The hydrology models are run for each GCM–radiative forcing for the historical runs (1861-2005) and two greenhouse gas concentration scenarios (low greenhouse gas concentration scenario for RCP2.6; medium–high greenhouse gas concentration scenario for RCP 6.0) for future projections (2006-2099). Meteorological forcing data (precipitation, air temperature, solar radiation, wind speed, specific humidity, and surface pressure) were bias-adjusted[38] to EWEMBI data set and downscaled to 0.5° × 0.5° spatial resolution using an updated version of the Fast-Track methods[21,41]. Most GHMs (except CLM4.5) in ISMIP2b considered varying water abstraction and land use according to SSP2 and RCP2.6 (RCP6.0). The influences of human activities are time varying in historical periods (1850–2015) but constant in the future (e.g., fixed year-2005 dams and reservoirs)[22]. Although ISIMIP2b considered 1861–2005 as the historical period and 2006–2100 as the future, we treated 1901–2020 as the historical one and 2021–2090 as the future when interpreting our results.

We used annual global population data at 0.5° × 0.5° resolution for 1901–2020 (historical period), obtained from the HYDE3.2 database[42]; for the future period, we used the shared socioeconomic pathways projections[43] (SSP2 and SSP3) defined by O'Neill et al. [44] These two datasets are employed in ISIMIP2b. However, there are discontinuities in the individual grid cells population time series, especially between 2005 and 2006. Therefore, we selected historical and scenario population at ten-year intervals and linearly interpolated them to yearly consistent population time series. The original sources for observations and projections of spatially-explicit population data differ in their spatial resolution and are independently calibrated. Hence, population values for specific grid points can vary significantly between observations and projections, even when smoothing the data with an 11-year window.

Although theoretically, each SSP could be combined with each RCP, some combinations of SSP and RCP are not expected to arise in the future due to their pronounced incompatibility[45]. Some studies[10,46] have focused on three RCP-SSP combinations: sustainability (RCP2.6-SSP1), fragmented world (RCP6.0-SSP3), and fossil fuel-based development (RCP8.5-SSP5). Here we considered four combinations: RCP2.6-SSP2, RCP2.6-SSP3, RCP6.0-SSP2, and RCP6.0-SSP3 to allow for flexibility in studying climate change and population growth trends.

### Calculation of FirstWS and EndWS

We used the threshold of 1000 $m^3$ per person per year to designate water scarcity, this being the Falkenmark water scarcity indicator[4,17,18]. This indicator is widely used to assess water scarcity, and although criticisms of its simplicity persist, its main strength is the limited input data requirement[47,48]. For each 0.5° grid cell, we calculated the first time water scarcity occurred (FirstWS) as the year when annual water availability first dipped below 1000 $m^3$ per person per year for at least

five consecutive years. Some regions may eventually experience a disappearance of water scarcity (e.g., driven by a decreasing population or increasing water availability), so we calculated the first time that water scarcity disappeared (EndWS), this being where per capita water availability exceeds 1000 $m^3$ per person per year and lasts until 2090. Thus, EndWS can only occur once for any given grid cell. The methodology for determining the FirstWS and EndWS is detailed in Supplementary Fig. 1.

The FirstWS and EndWS were assessed individually for each of the 24 different GHM-GCM combinations, and then the medians of that ensemble were calculated (Supplementary Fig. 26). To limit the effects of noise from natural climatic variation within and between years, we first calculated an 11-year moving average of water availability to identify the FirstWS and EndWS.

### Calculation of $A_{WS}$, $A_{FirstWS}$, and $A_{EndWS}$

Water scarcity area ($A_{WS}$) refers to the total land area where per capita water availability falls below the threshold of 1000 $m^3$ water per person per year in a given year. To further characterize the onset of water scarcity, we computed the area of regions where the per capita water availability first dropped below this threshold and remained below it for at least five consecutive years. This quantity is denoted as $A_{FirstWS}$ and represents the total area of regions that experienced prolonged water scarcity for the first time in a given year.

We performed the following steps for each grid cell to obtain annual water scarcity estimates. Firstly, we assessed if the cell was in a state of water scarcity and marked it accordingly. We then calculated the area of each marked cell that experienced water scarcity. Subsequently, we spatially aggregated the marked cells to national, subcontinental, and global levels each year. This produced an annual time series for each level of aggregation covering the period from 1901 to 2090.

For each year and cell of the time series, we performed an iterative process to identify the occurrence of FirstWS or EndWS. Subsequently, we assigned appropriate identifiers to these cells. To obtain the total area affected by water scarcity, we summed up the areas of all grid cells marked as such.

Additionally, we computed the areas corresponding to FirstWS and EndWS by adding up the grid cell areas where these events were identified. This yielded the values of $A_{FirstWS}$ and $A_{EndWS}$, respectively. Finally, we obtained the value of $A_{WS}$ by summing up the areas affected by water scarcity, FirstWS, and EndWS.

### Trends in population, water availability, and water availability per capita

The trends (β) in the population (Supplementary Fig. 15), water availability (Supplementary Fig. 12), and water availability per capita (Supplementary Fig. 6) over time were calculated using the Theil-Sen slope[49]. The statistical significance (p values) of those time series was estimated by a nonparametric trend test (Mann–Kendall test)[50]. We firstly calculated the mean water availability of 24 GHM-GCM combinations, and then calculated the trends under the four RCP-SSP scenario combinations.

### Sensitivity analysis

We tested the sensitivity of FirstWS to four factors. Firstly, the median of the 24 GHM-GCM combinations can be used to estimate FirstWS in different ways. Here we calculated FirstWS for each grid cell from each of the 24 different GHM-GCM combinations and then took the median of these 24 FirstWS estimates. An alternative approach would be first to obtain the mean water availability from the 24 GHM-GCM combinations and then estimate FirstWS using the mean water availability data. To explore whether selecting this alternative approach would influence the estimates of FirstWS, we compared both approaches and found a similar spatial pattern (Fig. 2; Supplementary Fig. 20).

Secondly, the time length of the window used to estimate the moving averages of water availability may influence the FirstWS. Accordingly, we also tested its sensitivity to this by applying 5-year and 21-year windows. For the same threshold of 1000 $m^3$ per person per year, the FirstWS with 5-year, 11-year, and 21-year moving averages all featured similar results globally, albeit with a few regional differences (Fig. 2; Supplementary Fig. 21), thus indicating the robustness of our estimates.

Thirdly, the threshold for defining water scarcity can also influence the WS. According to Falkenmark[4,51], an area is experiencing water stress when annual water supplies drop below 1700 $m^3$ per person. When annual water supplies drop below 1000 $m^3$ per person, the population faces water scarcity, and when it falls below 500 cubic meters, it signifies absolute scarcity. Besides 1000 $m^3$, we also tested 500 $m^3$ (extreme water scarcity) and 1700 $m^3$ (water stress) to assess and discuss the sensitivity in the FirstWS estimates (Supplementary Fig. 22).

Fourthly, we tested the sensitivity of FirstWS on grid and watershed scale. Besides the 0.5° grid cell, we repeated our analysis using the level-04 global watershed definitions by HydroBASINS, which consists of 1276 watersheds[52]. We first aggregated the watershed-scale runoff and population, calculated the water availability per capita of each watershed, and then obtained FirstWS of each watershed (Fig. 2 vs. Supplementary Fig. 23).

Finally, the uncertainty of our two indicators might arise from data uncertainty. We used the other runoff data (G-RUN ensemble[28] between 1902 and 2019) to test the validity of our data sources (Supplementary Fig. 24). Considering that there is little EndWS before 2020, we only compared the consistency of FirstWS between 24 GHMs-GCMs combinations and G-RUN[28] ensemble mean runoff. The G-RUN ensemble[28] runoff was created through machine learning and a global collection of river discharge observations, thus can be seen as the benchmark of the ISIMIP2b-derived runoff. Besides, the uncertainty of total runoff among the four GCMs and six GHMs was further tested. We reorganized the ISIMIP2b-derived runoff according to GCMs types or GHMs types (Supplementary Fig. 18). The six GHMs (here fix the GCMs by averaging four GCMs) have large uncertainties, but the four GCMs (here fix the GHMs by averaging six GHMs) have relatively low uncertainties compared to that of six GHMs (Supplementary Fig. 18). Despite the large uncertainty of total runoff among different GCMs and GHMs, we found the overall consistent distribution of FirstWS among GCMs but with a large difference among six GHMs (Supplementary Fig. 25). Despite the discrepancies among different models, we used the multi-model ensemble median of 24 FirstWS to minimize the uncertainties caused by these discrepancies.

## Data availability

All datasets are freely accessible to the public from these locations. The global grid water availability data from ISIMIP2b is available online from https://data.isimip.org/search/tree/ISIMIP2b/OutputData/water_global/. Annual global grid population (SSP2 and SSP3) data is also available from ISIMIP: https://www.isimip.org/gettingstarted/input-data-bias-correction/. The global watershed boundaries come from HydroBASINS at the level-04 (https://www.hydrosheds.org/products/hydrobasins).

## Code availability

The data and figures in this study were produced with MATLAB 9.10 (R2021a), which used built-in functions in MATLAB and other publicly available tool packages. The publicly available tool packages includes: *ktaub*.m (https://www.mathworks.com/matlabcentral/fileexchange/11190-mann-kendall-tau-b-with-sen-s-method-enhanced), *nanfastsmooth.m* (https://ww2.mathworks.cn/matlabcentral/fileexchange/52688-nan-tolerant-fast-smooth), *boundedline.m* (https://ww2.mathworks.cn/matlabcentral/fileexchange/27485-boundedline-m).

The code used to correct population consistency between historical and future periods was provided through the GitHub repository at https://github.com/VUB-HYDR/isimip2b_population_correction.

## References


1. WEF. Global Risks Report 2020, 15th Edition. (World Economic Forum, Geneva, 2020).
2. Vörösmarty, C. J., Pahl-Wostl, C., Bunn, S. E. & Lawford, R. Global water, the anthropocene and the transformation of a science. *Curr. Opin. Environ. Sustain* **5**, 539–550 (2013).
3. Liu, J. et al. On knowledge generation and use for sustainability. *Nat. Sustain* **2**, 80–82 (2019).
4. Falkenmark, M. et al. Macro-scale water scarcity requires micro-scale approaches. *Nat. Res. Forum* **13**, 258–267 (1989).
5. Gosling, S. N. & Arnell, N. W. A global assessment of the impact of climate change on water scarcity. *Clim. Chang* **134**, 371–385 (2016).
6. Elliott, J. et al. Constraints and potentials of future irrigation water availability on agricultural production under climate change. *Proc. Natl Acad. Sci. USA* **111**, 3239–3244 (2014).
7. Prudhomme, C. et al. Hydrological droughts in the 21st century, hotspots and uncertainties from a global multimodel ensemble experiment. *Proc. Natl Acad. Sci. USA* **111**, 3262–3267 (2014).
8. Haddeland, I. et al. Global water resources affected by human interventions and climate change. *Proc. Natl Acad. Sci. USA* **111**, 3251–3256 (2014).
9. Schewe, J. et al. Multimodel assessment of water scarcity under climate change. *Proc. Natl Acad. Sci. USA* **111**, 3245–3250 (2014).
10. Veldkamp, T. I. E., Wada, Y., Aerts, J. C. J. H. & Ward, P. J. Towards a global water scarcity risk assessment framework: incorporation of probability distributions and hydro-climatic variability. *Environ. Res. Lett.* **11**, 024006 (2016).
11. Mekonnen, M. M. & Hoekstra, A. Y. Four billion people facing severe water scarcity. *Sci. Adv.* **2**, e1500323 (2016).
12. Kummu, M. et al. The world's road to water scarcity: shortage and stress in the 20th century and pathways towards sustainability. *Sci. Rep.* **6**, 38495 (2016).
13. He, C. et al. Future global urban water scarcity and potential solutions. *Nat. Commun.* **12**, 4667 (2021).
14. Greve, P. et al. Global assessment of water challenges under uncertainty in water scarcity projections. *Nat. Sustain* **1**, 486–494 (2018).
15. Satoh, Y. et al. The timing of unprecedented hydrological drought under climate change. *Nat. Commun.* **13**, 3287 (2022).
16. Damkjaer, S. & Taylor, R. The measurement of water scarcity: Defining a meaningful indicator. *Ambio* **46**, 513–531 (2017).
17. Falkenmark, M. et al. On the Verge of a New Water Scarcity: A Call for Good Governance and Human Ingenuity. (SIWI Policy Brief, 2007).
18. Falkenmark, M. Growing water scarcity in agriculture: future challenge to global water security. *Philos. Trans. R. Soc. A* **371**, 1–14 (2013).
19. Gleick, P. H. & Cooley, H. Freshwater Scarcity. *Annu. Rev. Env. Resour.* **46**, 319–348 (2021).
20. Liu, J. et al. Water scarcity assessments in the past, present, and future. *Earth's Future* **5**, 545–559 (2017).
21. Frieler, K. et al. Assessing the impacts of 1.5 °C global warming—simulationprotocol of the Inter-Sectoral Impact Model Intercomparison Project (ISIMIP2b). *Geosci. Model Dev.* **10**, 4321–4345 (2017).
22. Gudmundsson, L. et al. Globally observed trends in mean and extreme river flow attributed to climate change. *Science* **371**, 1159–1162 (2021).
23. Ju, J. et al. Global evaluation of model agreement and uncertainty in terrestrial water storage simulations from ISIMIP 2b framework. *J. Hydrol.* **617**, 129137 (2023).
24. Porkka, M. et al. Notable shifts beyond pre-industrial streamflow and soil moisture conditions transgress the planetary boundary for freshwater change. *Nat. Water*. **2**, 262–273 (2024).
25. Wang et al. Anthropogenic climate change has influenced global river flow seasonality. *Science* **383**, 1009–1014 (2024).
26. Newman, A. J. et al. Development of a large-sample watershed-scale hydrometeorological data set for the contiguous USA: data set characteristics and assessment of regional variability in hydrologic model performance. *Hydrol. Earth Syst. Sci.* **19**, 209–223 (2015).
27. Greve, P. et al. Global assessment of trends in wetting and drying over land. *Nat. Geosci.* **7**, 716–721 (2014).
28. Ghiggi, G., Humphrey, V., Seneviratne, S. I. & Gudmundsson, L. G-RUN ENSEMBLE: A Multi-Forcing Observation-Based Global Runoff Reanalysis. *Wat. Resour. Res* **57**, e2020WR028787 (2021).
29. Pokhrel, Y. et al. Global terrestrial water storage and drought severity under climate change. *Nat. Clim. Change* **11**, 226–233 (2021).
30. Gurung, K. et al. Climate windows of opportunity for plant expansion during the Phanerozoic. *Nat. Commun.* **13**, 4530 (2022).
31. Rogelj, J. et al. A new scenario logic for the Paris Agreement long-term temperature goal. *Nature* **573**, 357–363 (2019).
32. Sadoff, C. W., Borgomeo, E. & Uhlenbrook, S. Rethinking water for SDG 6. *Nat. Sustain* **3**, 346–347 (2020).
33. Long, K. & Pijanowski, B. C. Is there a relationship between water scarcity and water use efficiency in China? A national decadal assessment across spatial scales. *Land Use Policy* **69**, 502–511 (2017).
34. Thompson, J. R., Gosling, S. N., Zaherpour, J. & Laizé, C. L. R. Increasing risk of ecological change to major rivers of the world with global warming. *Earth's Future* **9**, e2021EF002048 (2021).
35. Jasechko, S. & Perrone, D. Global groundwater wells at risk of running dry. *Science* **372**, 418–421 (2021).
36. Liu, X. et al. Environmental flow requirements largely reshape global surface water scarcity assessment. *Environ. Res. Lett.* **16**, 104029 (2021).
37. Vanham, D. et al. The number of people exposed to water stress in relation to how much water is reserved for the environment: a global modelling study. *Lancet Planet. Health* **5**, e766–e774 (2021).
38. Covey, C. et al. An overview of results from the Coupled Model Intercomparison Project. *Glob. Planet. Change* **37**, 103–133 (2003).
39. Veldkamp, T. et al. Water scarcity hotspots travel downstream due to human interventions in the 20th and 21st century. *Nat. Commun.* **8**, 1–12 (2017).
40. Zhao, X. et al. Physical and virtual water transfers for regional water stress alleviation in China. *Proc. Natl Acad. Sci. USA* **112**, 1031–1035 (2015).
41. Lange, S. Trend-preserving bias adjustment and statistical downscaling with ISIMIP3BASD (v1.0). *Geosci. Model Dev.* **12**, 3055–3070 (2019).
42. Klein Goldewijk, K., Beusen, A., Doelman, J. & Stehfest, E. Anthropogenic land use estimates for the Holocene – HYDE 3.2. *Earth Syst. Sci. Data* **9**, 827–953 (2017).
43. Jones, B. & O'Neill, B. Spatially explicit global population scenarios consistent with the Shared Socioeconomic Pathways. *Environ. Res. Lett.* **11**, 084003 (2016).
44. O'Neill, B. C. et al. The Scenario Model Intercomparison Project (ScenarioMIP) for CMIP6. *Geosci. Model Dev.* **9**, 3461–3482 (2016).
45. Arnell, N. W. & Lloyd-Hughes, B. The global-scale impacts of climate change on water resources and flooding under new climate and socioeconomic scenarios. *Clim. Chang* **122**, 127–140 (2014).
46. Winsemius, H. C. et al. Global drivers of future river flood risk. *Nat. Clim. Change* **6**, 381–385 (2016).
47. Brown, A. & Matlock, M. D. A review of water scarcity indices and methodologies. *White Pap.* **106**, 19 (2011).
48. Rijsberman, F. R. Water scarcity: fact or fiction? *Agric. Water Manag.* **80**, 5–22 (2006).

49. Sen, K. P. Estimates of the Regression Coefficient Based on Kendall's Tau. *J. Am. Stat. Assoc.* **63**, 1379–1389 (1968).
50. Hirsch, R. M., Slack, J. R. & Smith, R. A. Techniques of trend analysis for monthly water quality data. *Water Resour. Res.* **18**, 107–121 (1982).
51. Vanham, D., Alfieri, L. & Feyen, L. National water shortage for low to high environmental flow protection. *Sci. Rep.* **12**, 3037 (2022).
52. Lehner, B. & Grill, G. Global river hydrography and network routing: baseline data and new approaches to study the world's large river systems. *Hydrol. Process.* **27**, 2171–2186 (2013).

## Acknowledgements

This study has been supported by the National Natural Science Foundation of China (grant no. 42361144001, no. 41625001), Henan Provincial Key Laboratory of Hydrosphere and Watershed Water Security, the Strategic Priority Research Program of the Chinese Academy of Sciences (grant no. XDA20060402). MK was financially supported by the European Research Council (ERC) under the European Union's Horizon 2020 research and innovation program (grant agreement no. 819202) and Research Council of Finland's Flagship Programme under project Digital Waters (grant no. 359248). PC acknowledges support from the ANR CLAND Convergence Institute. We also thank Dr. Peter H. Gleick from the Pacific Institute and Dr. Karim C. Abbaspour from 2w2e Environmental Consulting GmbH for their advice on revising the paper.

## Author contributions

J.L. conceived the work. D.L. collected data, performed the calculations and statistical analyses, and prepared the tables and figures. J.L. and D.L. worked on the first draft of the manuscript. H.C, H.W., Y.W., M.K., S.N.G., H.Y., Y.P. and P.C. contributed to the data interpretation as well as the preparation of the manuscript's text.

## Competing interests

The authors declare no competing interests.

## Additional information

**Supplementary information** The online version contains supplementary material available at https://doi.org/10.1038/s41467-024-51302-z.

**Correspondence** and requests for materials should be addressed to Junguo Liu.

**Peer review information** *Nature Communications* thanks the anonymous reviewers for their contribution to the peer review of this work. A peer review file is available.